Dalton Transactions

Salt Loading in MOFs: Solvent-Free and Solvent-Assisted Loading of NH_4NO_3 and $LiNO_3$ in UiO-66

Journal:	*Dalton Transactions*
Manuscript ID	DT-ART-06-2019-002489.R2
Article Type:	Paper
Date Submitted by the Author:	08-Aug-2019
Complete List of Authors:	Seth, Saona; University of Michigan, Ann Arbor, Chemistry Vaid, Thomas; University of Michigan, Chemistry Matzger, Adam; University of Michigan, Chemistry

SCHOLARONE™
Manuscripts

Please do not adjust margins

ARTICLE

Salt Loading in MOFs: Solvent-Free and Solvent-Assisted Loading of NH_4NO_3 and $LiNO_3$ in UiO-66

Received 00th January 20xx,
Accepted 00th January 20xx

DOI: 10.1039/x0xx00000x

Saona Seth,[a] Thomas P. Vaid,[a] and Adam J. Matzger[a,b]*

While the loading of liquid or solid materials in the pores of metal-organic frameworks (MOFs) can yield composite materials with novel and useful emergent properties, the loading of solids, and ionic solids in particular, can be challenging. We report the loading of the salts NH_4NO_3 and $LiNO_3$ in the MOF UiO-66. The relatively low-melting NH_4NO_3 is loaded in UiO-66 in a solvent-free method, and loading is complete in 8 h at 75 °C, far below the melting point of NH_4NO_3. The higher-melting $LiNO_3$ requires a small amount of solvent (water) for loading, and active removal of water assists in loading of the salt to form a composite that is 38 % by mass $LiNO_3$. These and similar salt-MOF composites are of interest for applications such as solid-ion conductors and energetic materials.

Introduction

Guest inclusion in metal-organic frameworks (MOFs) is central to their application in gas storage, molecular separations, and catalysis. The relatively large pores and apertures joining the pores in MOFs (compared to zeolites, the other common class of crystalline microporous materials) usually present a low kinetic barrier to the entry of molecular gases and liquids. Molecular or ionic solids, however, cannot directly enter the interior of a MOF. Nonetheless, new and potentially useful emergent properties are expected from the inclusion of a solid in the nanometer-scale pores of a MOF. For example, disrupting the long-range structure of a salt in a MOF will enforce disorder in the lattice and create a large number of defects that should enhance ion mobility. A demonstration of enhanced ionic conductivity has been observed in LiI loaded in mesoporous alumina.[1,2] In another application, a MOF host could be loaded with an inorganic oxidizing salt to create an intimate mixture of fuel (the MOF) and oxidizer, which would be an energetic composite capable of rapid reaction, as in the loading of NH_4NO_3 in UiO-66, shown schematically in Fig. 1. Our group has previously reported the loading of molecular organic oxidizers in MOF-5, which leads to highly sensitive (primary) explosives.[3] By contrast, explosives that incorporate inorganic oxidizers (salts with positive oxygen balance) are expected to be impact-insensitive and thermally stable.

The loading of ionic solids in MOFs presents some challenges beyond those encountered in loading other solid or liquid materials in MOFs. After a MOF is synthesized, it is usually "activated" by removing the synthesis solvent(s), often by exchange with a solvent with lower surface tension followed by application of heat and/or vacuum.[4] Activation leaves the MOF framework in a relatively high-energy state due to the surface

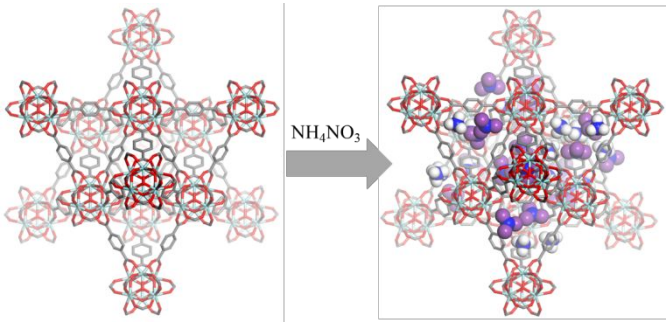

Fig. 1 Schematic representation of loading NH_4NO_3 in UiO-66 illustrating the relative size of the host and guest.

energy of the large internal surface of the MOF (up to several thousand m^2/g).[5] That surface energy provides the driving force that leads to the facile adsorption of most liquids into a MOF,[6,7] as long as the pores and apertures of the MOF are large enough to admit the molecules of the liquid. Only an extremely high surface tension liquid such as mercury (surface tension = 486 mN/m) will fail to be absorbed in most MOFs. (Studies have used liquid mercury as a medium to apply pressure to MOFs, specifically because mercury will *not* enter the pores of the MOF, even under high pressure.[8,9]) This facile liquid loading can be used to load molten solids in MOFs if the solid melts below the decomposition temperature of the MOF. This method is applicable as well to ionic species that are liquid or low-melting solids. Salts that are liquid at ambient temperatures or that melt below 100 °C are called "ionic liquids," and there is an extensive literature reporting the loading of ionic liquids in

[a] *Department of Chemistry, University of Michigan, 930 North University Avenue, Ann Arbor, Michigan 48109, United States.*
[b] *Macromolecular Science and Engineering Program, University of Michigan, 930 North University Avenue, Ann Arbor, Michigan 48109, United States.*

† Footnotes relating to the title and/or authors should appear here.
Electronic Supplementary Information (ESI) available: nitrogen sorption isotherm of activated UiO-66, SEM images and elemental mapping of NH_4NO_3-UiO-66 and $LiNO_3$-UiO-66 physical mixtures and composites, details concerning the energetic properties of NH_4NO_3-UiO-66 and $LiNO_3$-UiO-66, and a high-speed video of the detonation of the $LiNO_3$-UiO-66 composite. See DOI: 10.1039/x0xx00000x

Please do not adjust margins

MOFs.[10,11] The surface tension of most ionic liquids[12] falls in the range of ~30-50 mN/m (compare to water at 72 and benzene at 28 mN/m), so that does not present an obstacle to loading in MOFs. In fact, even traditional ionic salts have only moderate surface tension when molten; NaCl, for example, has a surface tension of 106 mN/m at 908 °C.[13] We have utilized this strategy for loading NH_4NO_3 (m.p. = 170 °C) in UiO-66, as described below.

When a salt does not melt at a temperature compatible with the MOF into which it is to be loaded, a solvent must be used. The introduction of a solvent as another component to the system makes the loading of the salt less likely to be thermodynamically favourable because the high surface energy of the interior of the MOF can be reduced by adsorption of the solvent, rather than the salt. Nevertheless, when there are favourable relative interaction energies (MOF-solute and solvent-solvent strong compared to MOF-solvent and solute-solute), loading of MOFs from saturated solutions has been possible both for neutral molecular solids and for salts. For example, we have previously demonstrated loading of dibenzothiophene and similar organosulfur molecules in several MOFs from solutions in isooctane[14] and two pharmaceuticals in MIL-100 from aqueous solution.[15] High-melting salts have also been successfully loaded from solution in MOFs, but it is relatively rare. Two examples are the loading of CuI from acetonitrile solution into a derivatized UiO-67[16] and the loading of $CaCl_2$ from aqueous solution into water-stable MIL and UiO MOFs.[17] When less forcing conditions are used (e.g., suspension of UiO-66 in 0.5 M $LiNO_3$ in ethanol), generally only modest loadings are obtained (less than 1:25 Li:Zr atomic ratio in that case).[18] A patent describes the loading of NH_4ClO_4 and NH_4NO_3 in MOFs from saturated solutions in either DMF or water.[19] However, no quantification of the amount of salt incorporated was provided, and the product was a physical mixture that included unloaded salt. In work motivated by the desire for solid-ion conductors for cations such as Li^+ and Mg^{2+}, MOFs were rendered anionic by the coordination of anions to the metal atoms of the MOF framework, leaving the cations (Li^+, Mg^{2+}, etc.) mobile.[20–23] However, in most of those materials residual solvent such as propylene carbonate or ethylene carbonate was present in the composite materials. Similarly, $LiClO_4$ in propylene carbonate has been adsorbed in HKUST-1, leading to a composite with the stoichiometry $Cu_3(BTC)_2(LiClO_4)_{2.8}(PC)_{4.6}$ (BTC = 1,3,5-benzenetricarboxylate; PC = propylene carbonate).[24] To examine and interpret physical properties such as ion mobility in MOF-salt composites, it would be advantageous to obtain materials that consist solely of the MOF and salt. The methods described herein lead to such simple composites.

When loading of a molecular solute from solution is not favourable, slow evaporation of the solvent can drive the loading. This strategy has been successfully used in the loading of organic molecules in single crystals of MOFs for X-ray crystallographic analysis in the "crystalline sponge" method.[25] We are not aware of any reports of this procedure being used to load salts in MOFs, although in a somewhat related method, a suspension of MIL-101 in hexane was loaded with suspended aqueous droplets of H_2PtCl_6 of a volume calculated just to fill the pores of MIL-101 present.[26] As described below, we used the slow evaporation of an aqueous solution of $LiNO_3$ to load it in UiO-66.

Experimental

Caution: *No unplanned detonations occurred during the experiments with NH_4NO_3-UiO-66 and $LiNO_3$-UiO-66 composites. However, these are high-energy materials and might cause injury upon explosion if proper safety practices are not followed.*

Synthesis and Activation of UiO-66. UiO-66 was synthesized by a method previously reported in the literature.[27] Prior to activation, the compound was thoroughly washed with dimethylformamide (DMF) four times to remove unreacted starting materials. DMF was exchanged with ethanol for one day, during which time the supernatant was replaced by fresh ethanol five times. Finally, solvent was decanted, and the compound was activated by exposure to a dynamic vacuum (~10^{-2} Torr) at 90 °C for 18 hours on a MasterPrep apparatus (Quantachrome Instruments).

Nitrogen Sorption Measurement. Nitrogen sorption isotherms were measured a NOVA e-Series 4200 surface area analyzer (Quantachrome Instruments). N_2 (99.999%) was purchased from Cryogenic Gases and used as received. Sorption isotherms were analyzed by NOVAwin software. For each N_2 isotherm measurement, a glass sample cell was charged with ~100 mg sample and analyzed at 77 K. The results for UiO-66 are shown in the Supporting Information, Fig. S1, yielding a surface area of 1530 $m^2 \cdot g^{-1}$.

Powder X-ray Diffraction (PXRD). Room-temperature PXRD data were collected on a PANalytical Empyrean diffractometer in Bragg–Brentano geometry using Cu-Kα radiation (1.54187 Å) and operating at 45 kV and 40 mA. The incident beam was equipped with a Bragg-BrentanoHD X-ray optic using fixed slits/soller slits. The detector was a silicon-based linear position sensitive X'Celerator Scientific operating in 1-D scanning mode. The samples were finely ground to minimize preferred orientation and packed in the depression of a glass slide.

Variable Temperature and Isothermal Salt Loading PXRD. Variable temperature PXRD data were collected on a Rigaku SmartLab diffractometer using Cu-Kα radiation (λ = 1.54187 Å) and operating at 40 kV and 44 mA. Ground samples were placed on a glass cover slip on top of a copper block that was heated using a J-KEM Model 210 temperature controller with a cartridge heater. The setup was covered with a housing of Kapton to keep heat in but allow X-rays to penetrate. The spectra were collected in reflection mode using a point focus source (0.8 mm collimator) and a 2D Pilatus detector by scanning 2θ from 25° to 35° in a continuous mode at each 25 °C temperature interval. Powder patterns were processed using Jade 8 XRD Pattern Processing, Identification & Quantification analysis software.

Raman Spectroscopy. Raman spectra were obtained using a Renishaw inVia Raman microscope equipped with a 633 nm laser (35 mW laser power), 1200 lines/mm grating, 65 μm slit,

 This journal is © The Royal Society of Chemistry 20xx

and CCD detector. The instrument was calibrated using a silicon standard. Spectra were collected at extended scan mode in the wave number range 100-3600 cm^{-1}, and analyzed using the Wire 4.2 software package.

Differential Scanning Calorimetry (DSC). DSC experiments were carried out on TA Instrument Q10 differential scanning calorimeter. The instrument was calibrated using an indium standard. Precisely weighed samples were placed in Tzero™ hermetic aluminum pans and heated in the temperature range of 30 to 500 °C at a heating rate of 10 °C/min under nitrogen atmosphere.

Results and discussion

Solvent-free loading of NH_4NO_3 in UiO-66

For the initial study of salt-MOF composite formation, NH_4NO_3 was chosen as the salt because of its low melting point of 170 °C and its appreciable vapor pressure even at moderate temperatures (e.g., v.p. = 0.448 torr at 148 °C[28]). These properties make possible the loading of NH_4NO_3 in MOFs by diffusion of the salt as a melt, or at temperatures significantly below the melting point by vapor and/or mobilized solid transport. UiO-66 was chosen for initial studies because it exhibits very high thermal, water, and chemical stability.[29,30] The MOF contains $[Zr_6O_4(OH)_4(O_2CR)_{12}]$ clusters as 12-connected nodes that are linked by phenylene rings leading to a cubic structure with octahedral and tetrahedral cavities and a pore volume of 0.45 $cm^3\ g^{-1}$ (~ 55 % of unit cell volume).[31] The potential for hydrogen bonding interactions between the hydroxyl groups of the $[Zr_6O_4(OH)_4(O_2CR)_{12}]$ clusters and salt anions, in addition to coordination of the salt cations by the oxo groups of the $[Zr_6O_4(OH)_4(O_2CR)_{12}]$ clusters, may enhance the interaction strength between the MOF and salt and increase the likelihood of successful inclusion of the salts in the MOF. Additionally, UiO-66 exhibits a thermal decomposition temperature much higher than NH_4NO_3, which allows the loading of NH_4NO_3 in UiO-66 to be examined by thermogravimetric analysis (TGA).

To monitor loading of NH_4NO_3 in UiO-66, a 1:3 w/w salt-MOF mixture was ground together and then heated from 25 °C to 100 °C in 25 °C increments, with the PXRD pattern recorded at each increment. Fig. 2 shows the PXRD pattern of the mixture/composite at each temperature, along with the PXRD pattern of UiO-66 at 25 °C (which does not change significantly with temperature) and the pattern for neat NH_4NO_3 at each temperature. Pure NH_4NO_3 undergoes two polymorphic phase transitions at 32 °C (IV to III) and 84 °C (III to II), or can undergo a direct transition from phase IV to II at about 52 °C,[32] so its PXRD pattern is shown at each temperature for comparison. Our PXRD patterns of neat NH_4NO_3 match the reported ones for the appropriate polymorphs at various temperatures,[33] although the pattern at 50 °C shows an incomplete conversion from polymorph IV to polymorph III, which is complete at 75 °C. At 25 °C, the PXRD pattern of the ground mixture displays peaks corresponding to both pristine UiO-66 and (polymorph IV) NH_4NO_3. At 50 °C, the PXRD pattern of neat NH_4NO_3 is that of polymorph III, although the conversion is not quite complete. This is not too surprising, as the temperature of the polymorphic phase transitions of NH_4NO_3 can depend on the history of the sample and can exhibit significant hysteresis,[32,34]

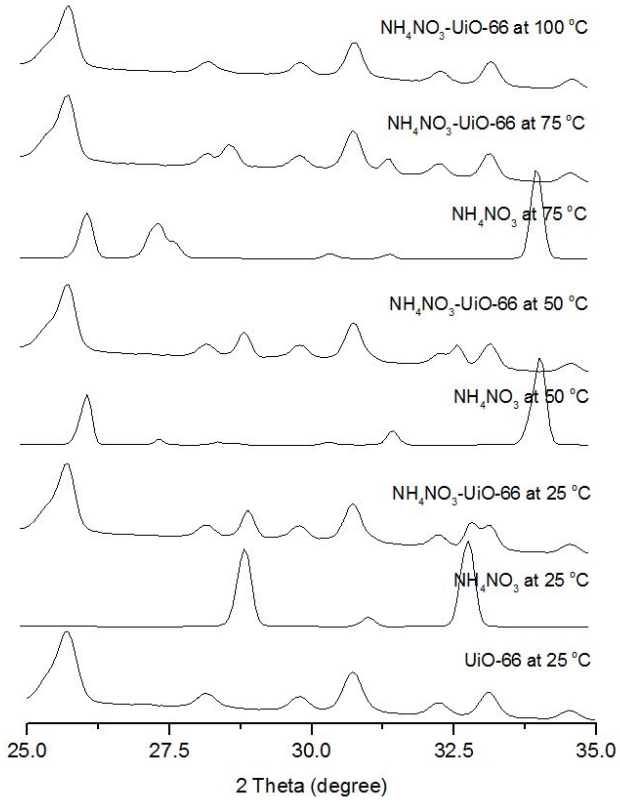

and the

Fig. 2 PXRD patterns of a 1:3 w/w mixture of NH_4NO_3 and UiO-66 at temperatures from 25 to 100 °C, along with the PXRD pattern of pristine UiO-66 at 25 °C and pure NH_4NO_3 at several temperatures.

grinding and presence of UiO-66 may have affected the transition temperature and/or rate. At 75 °C new peaks at 2θ = 27-27.5° appear in the PXRD pattern of neat NH_4NO_3 due the completed transition to polymorph III of NH_4NO_3. At 75 °C the PXRD pattern of the UiO-66-NH_4NO_3 mixture shows peaks due to UiO-66 and also some due to both polymorph IV and III of NH_4NO_3. Finally, at 100 °C the PXRD pattern of the UiO-66-NH_4NO_3 mixture shows only peaks due to UiO-66, indicating that all of the NH_4NO_3 has been absorbed into the pores of UiO-66, where the lack of long range order of the salt leads to its absence in the PXRD pattern. The full-profile PXRD patterns of NH_4NO_3, UiO-66, a physical mixture of the two, and the UiO-66-NH_4NO_3 composite are available in the ESI as Fig. S2.

To monitor the time course of diffusion of NH_4NO_3 in UiO-66, the salt-MOF mixture was isothermally heated at 75 °C, and the change in intensities of the salt peaks was monitored over time (Fig. 3). The salt peaks disappear completely after 8 h, suggesting complete inclusion of the salt in the MOF pores. This complete loading at 75 °C, far below the melting point of NH_4NO_3 (170 °C), indicates that either: 1) the ions of NH_4NO_3 are sufficiently mobilized at 75 °C that they are able to diffuse

directly into the MOF, or 2) some NH_4NO_3 is volatilized into the gas phase and is loaded into the MOF by that route. Alternatively, a UiO-66-NH_4NO_3 mixture can be heated to 175 °C (above the melting point of NH_4NO_3) to quickly effect complete absorption of the NH_4NO_3. Loading was accomplished by heating ground mixtures of NH_4NO_3 and UiO-66 in a capped vial, on scales from 10 mg to 100 mg NH_4NO_3.

Differential scanning calorimetry (DSC) measurements of the NH_4NO_3-UiO-66 composite provide further evidence of the loading of NH_4NO_3 in the MOF. Fig. 4 shows the DSC profile of pristine UiO-66, which has a small exothermic peak starting at about 325 °C, followed by a sharp endothermic peak, likely due to the dehydration of the MOF nodes to $[Zr_6O_6(O_2CR)_{12}]$, which occurs at 300 °C under vacuum.[30] The DSC trace of pure NH_4NO_3 shows two endothermic polymorphic phase transitions at 55 °C and 130 °C, slightly higher than the literature values of 52 °C and 125 °C for the IV → II and II → I transitions,[32] presumably due to the higher scan rate used in our experiments (10 °C/min vs. 2.5 °C/min). Those polymorphic transitions are followed by a melt endotherm at 170 °C, and finally an exothermic decomposition above 240 °C. In the DSC trace of the NH_4NO_3-UiO-66 composite, none of the NH_4NO_3 polymorphic phase transitions or melt is observed, due to the fact that the NH_4NO_3 lattice is completely disrupted within the MOF. The only feature observed in the NH_4NO_3-UiO-66 composite DSC is the exothermic decomposition at about 275 °C, indicating the possible utility of NH_4NO_3-UiO-66 as a relatively stable energetic/explosive material.

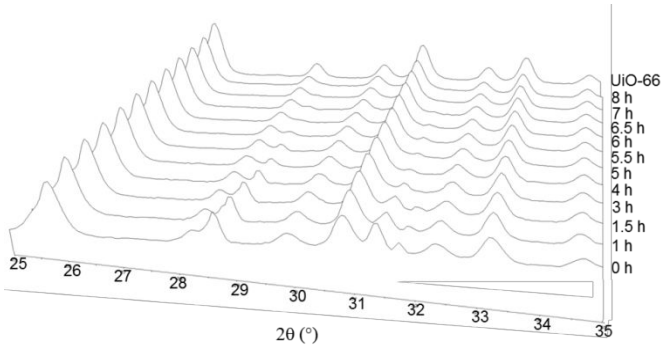

Fig. 3 Time evolution of the PXRD pattern of a mixture of NH_4NO_3 and UiO-66 at 75 °C, showing the uptake of NH_4NO_3 as evidenced from gradual disappearance of the salt peaks at 2θ = 28.7°, 31.4° and 31.7° over time.

TGA measurements on the NH_4NO_3-UiO-66 composite (Fig. 5) are consistent with the loading of NH_4NO_3. A mass loss of 32% occurs from about 150 °C to 190 °C due to evaporation of the NH_4NO_3, followed by decomposition of the UiO-66 host at about 500 °C. If a sample of the composite is heated to 220 °C and held at that temperature for several minutes to allow evaporation of the NH_4NO_3, subsequent PXRD analysis of the remaining material confirms that the UiO-66 framework has remained intact.

Inclusion of NH_4NO_3 in the pores of UiO-66 results in the shifting of the peak positions in the Raman spectra of both the framework and the NH_4NO_3 upon formation of the composite (Fig. 6 and Table 1).[30,34–36] For example, the peak from UiO-66 due to symmetric carboxylate stretching coupled with symmetric C–C stretching shifts from 1448 cm^{-1} to 1452 cm^{-1}. For NH_4NO_3, the symmetric stretching frequency of the nitrate in pristine NH_4NO_3 is shifted from 1043 cm^{-1} to 1047 cm^{-1} in the composite, while the nitrate antisymmetric bending mode at 715 cm^{-1} almost completely disappears. Hydrogen bonding between the NO_3^- anion and the OH groups of the $Zr_6O_4(OH)_4$ nodes of UiO-66 is one possible reason for the shifts in Raman band energy and intensity.

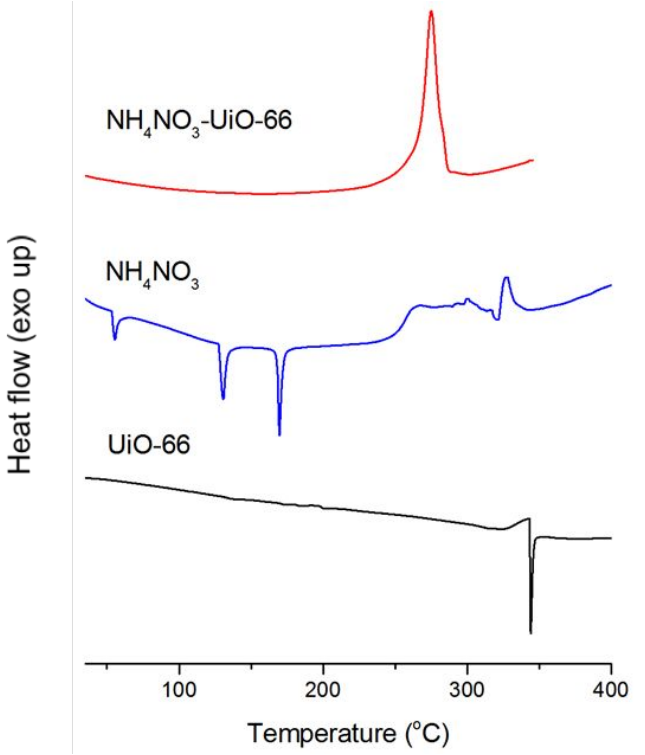

Fig. 4 DSC profile of NH_4NO_3-UiO-66 composite, pure NH_4NO_3, and pristine UiO-66.

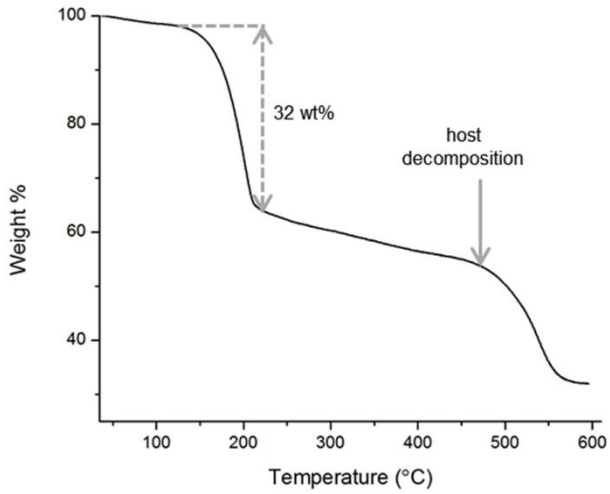

Fig. 5 TGA profile of the NH_4NO_3-UiO-66 composite.

The NH_4NO_3 loading in the MOF is also corroborated by SEM-EDS analyses data of the physical mixture of the salt and MOF and the resulting material obtained by heating the mixture at 100 °C. Elemental mapping of zirconium and nitrogen shows

This journal is © The Royal Society of Chemistry 20xx

Please do not adjust margins

presence of separate domains in the physical mixture that indicates an inhomogeneous dispersion of NH_4NO_3 and UiO-66. By contrast, the salt and MOFs are intimately mixed leading to homogeneous distribution of the elements in the composite (see Supporting Information, Figs. S3 and S4).

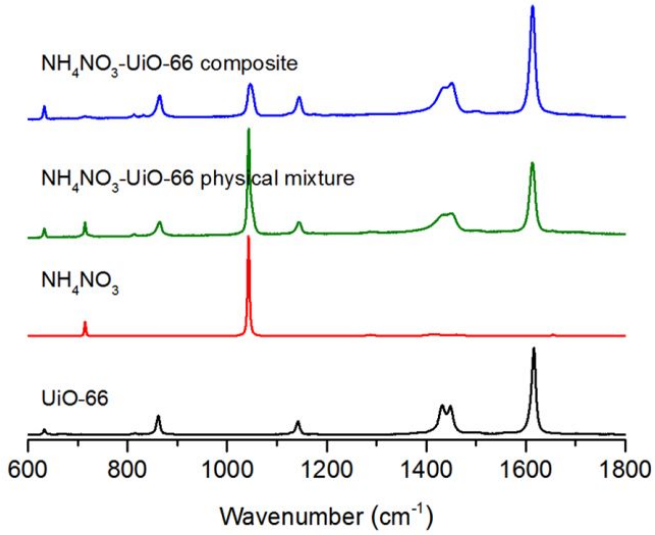

Fig. 6 Raman spectra of of NH_4NO_3-UiO-66 composite, a NH_4NO_3-UiO-66 physical mixture, pure NH_4NO_3, and pristine UiO-66.

Table 1 Raman frequencies (cm^{-1}) of UiO-66, NH_4NO_3, and the composite of the two components.

UiO-66	NH_4NO_3	composite
633		633
861		864
1142		1144
1433		1433
1448		1452
1616		1614
	715	-
	1043	1047

To determine the maximum amount of NH_4NO_3 loadable in UiO-66, the melt-diffusion experiment was carried out using varying amount of NH_4NO_3 with respect to the MOF, and heating the mixtures at 175 °C for ca. 8 h to ensure complete incorporation. PXRD analyses of the resulting materials indicate that up to 32 wt% loading of the salt with respect to the composite could be achieved. That can be compared to the theoretical value of 42.6 wt% NH_4NO_3 calculated based on 55 % void volume in UiO-66 and assuming NH_4NO_3 loads at the same density as pure NH_4NO_3. Because the NH_4NO_3 certainly cannot pack to fill all the void volume in UiO-66, the lower experimental loading is unsurprising. Subsequent experiments demonstrate that the diffusion rate of the molten salt at 175 °C is very fast with complete loading in less than 10 minutes.

Solvent-assisted loading of $LiNO_3$ in UiO-66

The loading of another salt, $LiNO_3$, was examined because of the interest in MOF composites as lithium-ion conductors.[20–23] However, melt loading of $LiNO_3$ without decomposition or reaction with the MOF is challenging because of the relatively high melting point of 255 °C of $LiNO_3$. Furthermore, vapour diffusion of $LiNO_3$ is not possible because of its extremely low vapour pressure even at elevated temperatures. Loading of $LiNO_3$ in UiO-66 was attempted by soaking the MOF in a continuously saturated aqueous solution of the salt for 1 h, and the resulting solid was isolated by filtration and vacuum drying.

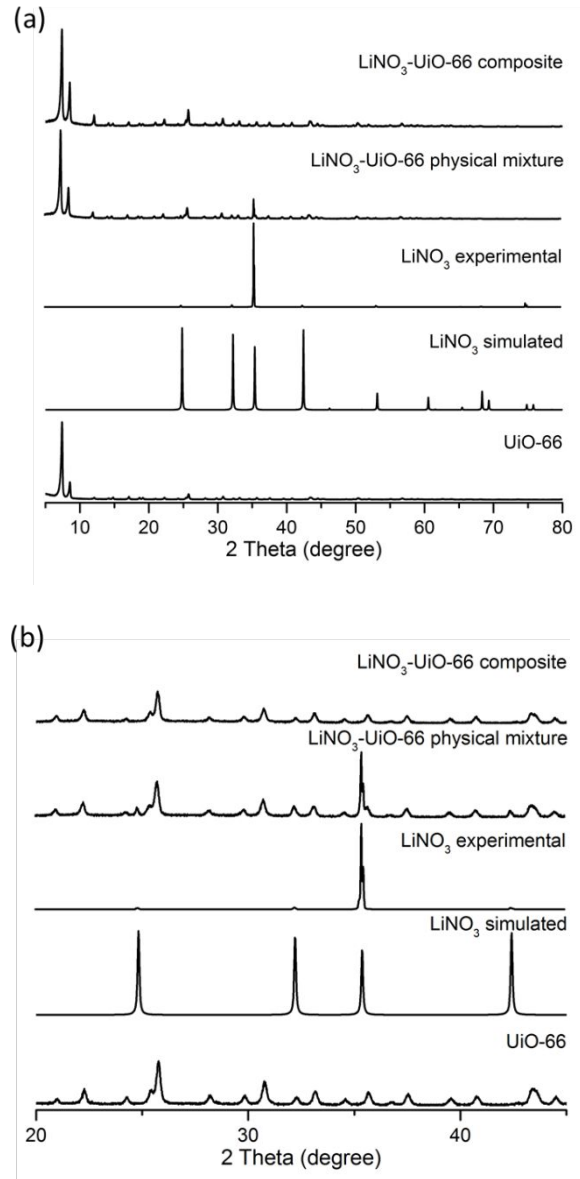

Fig. 7 (a) PXRD pattern of $LiNO_3$-UiO-66 composite in comparison with that of pristine UiO-66 and $LiNO_3$; (b) expanded PXRD profile for the 2θ range 20°-45°.

Analysis by PXRD revealed peaks corresponding to both MOF and salt, meaning that the salt is deposited, at least in part, on the MOF surface, rather than solely in the interior pores. To ensure that $LiNO_3$ is loaded in the MOF, solvent-assisted

diffusion of the salt was attempted using a controlled amount of the salt with respect to the MOF. Accordingly, 10 mg $LiNO_3$ was ground with 20 mg of UiO-66 and to the mixture was added deionized water (20 µL) to form a white paste. The mixture was held at 22 °C for 4 h in a capped 4 mL vial; subsequently, water was removed by heating at 100 °C for 1 h in an uncapped 4 mL vial open to the atmosphere. PXRD patterns of the samples after loading experiments match with that of UiO-66 (Fig. 7) with no additional peak that is characteristic of $LiNO_3$, indicating that the salt is present completely in the pores of UiO-66. Experiments with varying ratios of UiO-66 to $LiNO_3$ show that the $LiNO_3$-UiO-66 composite can be prepared with up to 38 wt% loading of $LiNO_3$; attempted loading with greater amounts of $LiNO_3$ showed residual crystalline $LiNO_3$ in the PXRD patterns (see Fig. S5 of ESI). In addition, the diminution in surface area of the MOF was proportional to the volume occupied by the salt—for example, a UiO-66 sample with surface area of 1098 $m^2 \cdot g^{-1}$ (determined by N_2 sorption) was loaded with 20 wt% $LiNO_3$ and its surface area decreased to 528 $m^2 \cdot g^{-1}$, roughly 18/38 of the original surface area (see Fig. S6 for the N_2 sorption isotherm). The theoretical fully loaded UiO-66 would be 50.6 wt% $LiNO_3$ if the salt loaded with the same density as pure $LiNO_3$. As with NH_4NO_3, it is not surprising that $LiNO_3$ does not fill the entire void volume within UiO-66.

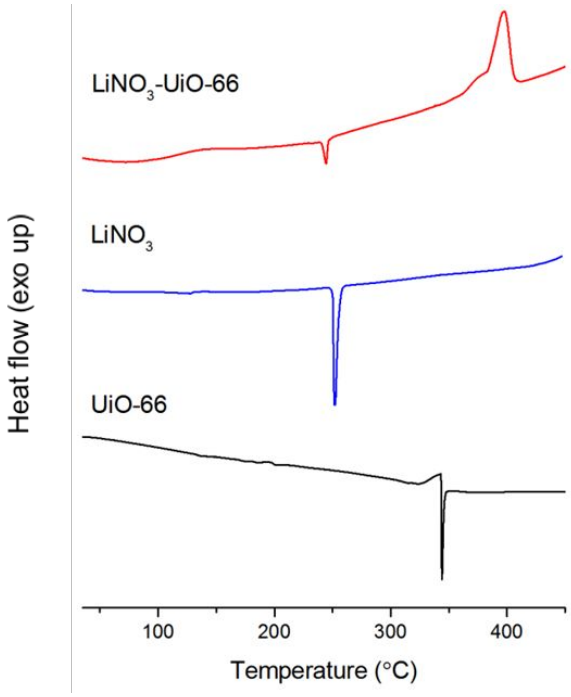

Fig. 8 DSC profile of $LiNO_3$-UiO-66 composite (38 wt% $LiNO_3$), pure $LiNO_3$, and pristine UiO-66.

The DSC profile of the $LiNO_3$-UiO-66 composite with 38 wt% $LiNO_3$ (Fig. 8) shows a greatly diminished melt endotherm for $LiNO_3$ at 255 °C. We believe this is due to a small amount of $LiNO_3$ that is still exterior to the MOF. Integration of the melt endotherm of the $LiNO_3$-UiO-66 composite indicates that it is only 4 % of the $LiNO_3$ present in the composite. While PXRD does not show any non-loaded $LiNO_3$ at this composition, DSC at all compositions inevitably showed a small amount of $LiNO_3$ external to the MOF. The DSC of the $LiNO_3$-UiO-66 composite shows an exothermic decomposition above 370 °C, presumably due to reaction between the MOF linkers and the oxidizing $LiNO_3$, indicating that the composite is a relatively stable energetic material. The TGA trace of the $LiNO_3$-UiO-66 composite (ESI, Fig. S7) shows some mass loss from 350-420 °C due to the same reaction/decomposition.

Loading of $LiNO_3$ was further confirmed by Raman spectroscopy (Fig. 9 and Table 2). The frequencies for symmetric carboxylate stretching coupled with symmetric C–C stretching of UiO-66 shifts from 1431 cm^{-1} to 1436 cm^{-1} and from 1448 cm^{-1} to 1453 cm^{-1}, in the composite. The sharp peak for symmetric nitrate stretching of $LiNO_3$ at 1069 cm^{-1} is decreased in intensity in the salt-MOF physical mixture and a new, broad peak at 1053 cm^{-1} appears. This broad peak persists in the composite obtained from solvent-assisted salt diffusion in the MOF, and the peak for the pristine $LiNO_3$ completely disappears. Finally, SEM-EDS analyses of the salt-MOF composite and the precursor salt-MOF mixture also support intimate mixing of oxidizer and fuel in the composite (see ESI, Figs. S8 and S9).

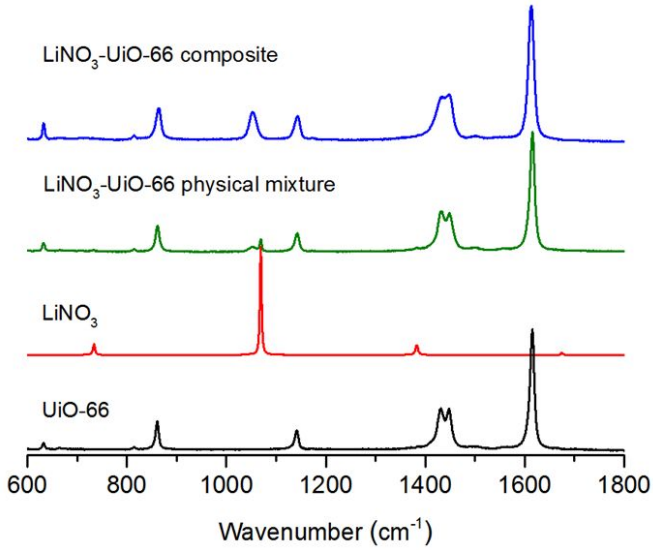

Fig. 9 Raman spectra of the $LiNO_3$-UiO-66 composite, a $LiNO_3$-UiO-66 physical mixture, pure $LiNO_3$, and pristine UiO-66.

Table 2 Raman frequencies (cm^{-1}) of UiO-66, $LiNO_3$, and the composite of the two

UiO-66	$LiNO_3$	composite
632		632
861		864
1142		1145
1431		1436
1448		1453
1616		1616
	734	-
	1069	1053
	1383	-

This journal is © The Royal Society of Chemistry 20xx

Conclusions

In conclusion, it is possible to achieve high mass loading of salts such as NH_4NO_3 and $LiNO_3$ in UiO-66 by solvent-free loading at elevated temperatures (for NH_4NO_3) or with the assistance of a minimal amount of solvent that is actively removed from the system (for $LiNO_3$). Such loading is often not achievable by a simple loading from a saturated solution, and has the advantage that there is no residual solvent in the final MOF-salt composite. The resultant MOF-salt composites may find use in a variety of applications, including solid ion conductors and composite energetic materials.

Conflicts of interest

There are no conflicts to declare.

Acknowledgements

This work was supported as part of the Joint Center for Energy Storage Research (JCESR), an Energy Innovation Hub funded by the U.S. Department of Energy, Office of Science, Basic Energy Sciences. Composites were discovered under a grant from the Defense Threat Reduction Agency (Grant HDTRA1-15-1-0001). We thank Dr. Kortney Kersten for assistance with variable temperature PXRD experiments.

Notes and references

‡ Footnotes relating to the main text should appear here. These might include comments relevant to but not central to the matter under discussion, limited experimental and spectral data, and crystallographic data.
§
§§

1 H. Maekawa, R. Tanaka, T. Sato, Y. Fujimaki and T. Yamamura, *Solid State Ionics*, 2004, **175**, 281–285.
2 H. Maekawa, Y. Fujimaki, H. Shen, J. Kawamura and T. Yamamura, *Solid State Ionics*, 2006, **177**, 2711–2714.
3 K. A. McDonald, J. C. Bennion, A. K. Leone and A. J. Matzger, *Chem. Commun.*, 2016, **52**, 10862–10865.
4 J. Ma, A. P. Kalenak, A. G. Wong-Foy and A. J. Matzger, *Angew. Chem. Int. Ed.*, 2017, **56**, 14618–14621.
5 K. Koh, A. G. Wong-Foy and A. J. Matzger, *Angew. Chem. Int. Ed.*, 2008, **47**, 677–680.
6 J. Rouquerol, F. Rouquerol, P. Llewellyn, G. Maurin and K. S. W. Sing, *Adsorption by Powders and Porous Solids: Principles, Methodology and Applications*, Academic Press, 2013.
7 S. Lowell, J. E. Shields, M. A. Thomas and M. Thommes, *Characterization of Porous Solids and Powders: Surface Area, Pore Size and Density*, Springer Science & Business Media, 2012.
8 I. Beurroies, M. Boulhout, P. L. Llewellyn, B. Kuchta, G. Férey, C. Serre and R. Denoyel, *Angew. Chem. Int. Ed.*, 2010, **49**, 7526–7529.
9 P. Yot, L. Vanduyfhuys, E. Alvarez, J. Rodriguez, J.-P. Itié, P. Fabry, N. Guillou, T. Devic, I. Beurroies, P. L. Llewellyn, V. V. Speybroeck, C. Serre and G. Maurin, *Chem. Sci.*, 2016, **7**, 446–450.
10 F. P. Kinik, A. Uzun and S. Keskin, *ChemSusChem*, 2017, **10**, 2842–2863.
11 K. Fujie and H. Kitagawa, *Coord. Chem. Rev.*, 2016, **307**, 382–390.
12 M. Tariq, M. G. Freire, B. Saramago, J. A. P. Coutinho, J. N. C. Lopes and L. P. N. Rebelo, *Chem. Soc. Rev.*, 2012, **41**, 829–868.
13 Y. Marcus, *Thermochim. Acta*, 2013, **571**, 77–81.
14 K. A. Cychosz, A. G. Wong-Foy and A. J. Matzger, *J. Am. Chem. Soc.*, 2008, **130**, 6938–6939.
15 K. A. Cychosz and A. J. Matzger, *Langmuir*, 2010, **26**, 17198–17202.
16 Y.-H. Hu, J.-C. Wang, S. Yang, Y.-A. Li and Y.-B. Dong, *Inorg. Chem.*, 2017, **56**, 8341–8347.
17 A. Permyakova, S. Wang, E. Courbon, F. Nouar, N. Heymans, P. D'Ans, N. Barrier, P. Billemont, G. D. Weireld, N. Steunou, M. Frère and C. Serre, *J. Mater. Chem. A*, 2017, **5**, 12889–12898.
18 Z. Niu, Q. Guan, Y. Shi, Y. Chen, Q. Chen, Z. Kong, P. Ning, S. Tian and R. Miao, *New J. Chem.*, 2018, **42**, 19764–19770.
19 United States, US8506734B1, 2013.
20 B. M. Wiers, M.-L. Foo, N. P. Balsara and J. R. Long, *J. Am. Chem. Soc.*, 2011, **133**, 14522–14525.
21 R. Ameloot, M. Aubrey, B. M. Wiers, A. P. Gómora-Figueroa, S. N. Patel, N. P. Balsara and J. R. Long, *Chem. Eur. J.*, 2013, **19**, 5533–5536.
22 S. S. Park, Y. Tulchinsky and M. Dincă, *J. Am. Chem. Soc.*, 2017, **139**, 13260–13263.
23 E. M. Miner, S. S. Park and M. Dincă, *J. Am. Chem. Soc.*, 2019, **141**, 4422–4427.
24 L. Shen, H. B. Wu, F. Liu, J. L. Brosmer, G. Shen, X. Wang, J. I. Zink, Q. Xiao, M. Cai, G. Wang, Y. Lu and B. Dunn, *Adv. Mater.*, 2018, **30**, 1707476.
25 Y. Inokuma, S. Yoshioka, J. Ariyoshi, T. Arai, Y. Hitora, K. Takada, S. Matsunaga, K. Rissanen and M. Fujita, *Nature*, 2013, **495**, 461–466.
26 A. Aijaz, A. Karkamkar, Y. J. Choi, N. Tsumori, E. Rönnebro, T. Autrey, H. Shioyama and Q. Xu, *J. Am. Chem. Soc.*, 2012, **134**, 13926–13929.
27 M. J. Katz, Z. J. Brown, Y. J. Colón, P. W. Siu, K. A. Scheidt, R. Q. Snurr, J. T. Hupp and O. K. Farha, *Chem. Commun.*, 2013, **49**, 9449–9451.
28 J. D. Brandner, N. M. Junk, J. W. Lawrence and J. Robins, *J. Chem. Eng. Data*, 1962, **7**, 227–228.
29 J. H. Cavka, S. Jakobsen, U. Olsbye, N. Guillou, C. Lamberti, S. Bordiga and K. P. Lillerud, *J. Am. Chem. Soc.*, 2008, **130**, 13850–13851.
30 L. Valenzano, B. Civalleri, S. Chavan, S. Bordiga, M. H. Nilsen, S. Jakobsen, K. P. Lillerud and C. Lamberti, *Chem. Mater.*, 2011, **23**, 1700–1718.
31 Q. Yang, A. D. Wiersum, P. L. Llewellyn, V. Guillerm, C. Serre and G. Maurin, *Chem. Commun.*, 2011, **47**, 9603–9605.
32 J. S. Ingman, G. J. Kearley and S. F. A. Kettle, *J. Chem. Soc., Faraday Trans. 1*, 1982, **78**, 1817–1826.
33 H. B. Wu, M. N. Chan and C. K. Chan, *Aerosol Sci. Technol.*, 2007, **41**, 581–588.
34 M. E. E. Harju, *Appl. Spectrosc.*, 1993, **47**, 1926–1930.
35 K. Tan, N. Nijem, P. Canepa, Q. Gong, J. Li, T. Thonhauser and Y. J. Chabal, *Chem. Mater.*, 2012, **24**, 3153–3167.

36 M. Ghosh, L. Wang and S. A. Asher, *Appl. Spectrosc.*, 2012, **66**, 1013–1021.

This journal is © The Royal Society of Chemistry 20xx

Please do not adjust margins

The salts NH_4NO_3 and $LiNO_3$ were loaded in the MOF UiO-66 by a solvent-free and solvent-assisted method, respectively.